Mater. Res. Soc. Symp. Proc. Vol. 1049 © 2008 Materials Research Society 1049-AA06-09

Instrumented Indentation Contact with Sharp Probes of Varying Acuity

Dylan J. Morris
Materials Science and Engineering Laboratory, National Institute of Standards and Technology, 100 Bureau Drive, MS 8520, Gaithersburg, MD, 20899

ABSTRACT

While elastic and plastic material property extraction from instrumented indentation tests has been well-studied, similarly-based fracture property measurement remains difficult. Furthermore, estimation of the fracture toughness requires measurement of the crack lengths from a micrograph, which makes nano-scale indentation toughness measurement expensive and difficult. Initiation and propagation of cracks on the nano-scale requires a more acute indenter than a Berkovich or sphere, such as the cube-corner pyramid. Experiments described here were performed on a range of elastic, plastic and brittle materials with diamond indenters of acuity varying between the Berkovich and the cube-corner. These experiments reveal some of what is changed and what remains the same, when the acuity of the probe is changed, when fracture is initiated at the contact, or both. A preliminary model for the physical origin of the extra crack-driving power of acute probes is presented in light of these, and complementary macro-scale *in-situ* indentation experiments. This work provides the basis for development of instrumented indentation-based nano-scale toughness measurement.

INTRODUCTION

Indentation by sharp diamond probes is a common procedure to investigate the elastic, plastic, viscous and fracture properties of materials in small volumes with little or no special sample preparation. Unfortunately, if fracture is to be studied, the frequently-used pyramidal Berkovich geometry rarely initiates fracture at loads common to nanoindentation, which are on the order of tens or hundreds of mN. The cube-corner indenter, a three-sided pyramid that is much more acute than the Berkovich, has been shown to be capable of reducing the load, and therefore the indentation length scale, needed to initiate radial fracture by several orders of magnitude [1, 2]. With knowledge of the elastic and plastic properties of the material, the crack lengths can be interpreted within the conventional model of indentation fracture to estimate the material toughness; for example, see the review by Cook and Pharr [3].

Essentially, the conventional model of indentation fracture asserts that constraint of the localized, irreversible plastic deformation zone causes an elastic reaction and accompanying tensile hoop stress at the material surface, which drives radial cracks. The reversible (not plastic) effect of indentation is to apply surface pressures; which, in classic indentation solutions such as those associated with Boussinesq, Love and Hertz, retard radial cracking with compressive surface hoop stresses outside the contacted zone. This elastic indentation + elastic-plastic model is sufficient to explain *in situ* transmission optical microscopy studies of crack growth during the indentation cycle for Vickers indentation, *e.g.* [4, 5].

Measurement of crack lengths at cube-corner indentations [2] *after* the indentation event seemed to confirm that the conventional elastic-plastic model of indentation fracture was obeyed when the indenter acuity was varied. That is, the crack lengths and the manner in which they scale with indentation load varied according to the scaling laws used in the conventional analysis. In fact, the cube-corner geometry appeared to be perform even better than Vickers or

Berkovich geometries when making toughness estimates; cube-corner indentation on the anomalous glasses fused silica and borosilicate glass obeyed the conventional indentation fracture model, whereas the fracture toughness of anomalous glasses is greatly overestimated from Vickers indentation [2]. The anomalous property of fused silica and borosilicate glass is their significant free volume, which allows them to compact underneath the pressures of indentation rather than plastically flow in a volume-conserving manner [6]. The competing deformation mechanism of compaction reduces the strength of the irreversible elastic-plastic field.

However, *in-situ* observation of radial crack growth during cube-corner indentation revealed that adherence to the conventional model was only coincidental [1]. The surprising effect of the reversible elastic field was to simultaneously drive and resist radial fracture, causing most crack growth to occur during loading with a weak contribution from the irreversible elastic-plastic field. This explains why it is possible to make good estimates of fracture toughness on the anomalous glasses with a cube-corner; plastic deformation is largely irrelevant to crack development. Later, a fracture-mechanics based indentation model described the reversible action of an acute indenter as a combination of a classic pressure-derived field and a crack-wedging field [7]. This model was successful at explaining much of the cube-corner indentation fracture phenomena [8], but the *ad hoc* mechanism of indentation wedging described there is unsatisfactory. In this work a potential explanation of indentation wedging phenomena is offered by appeal to experimental results from instrumented nanoindentation. The experiments are described below.

EXPERIMENTAL RESULTS

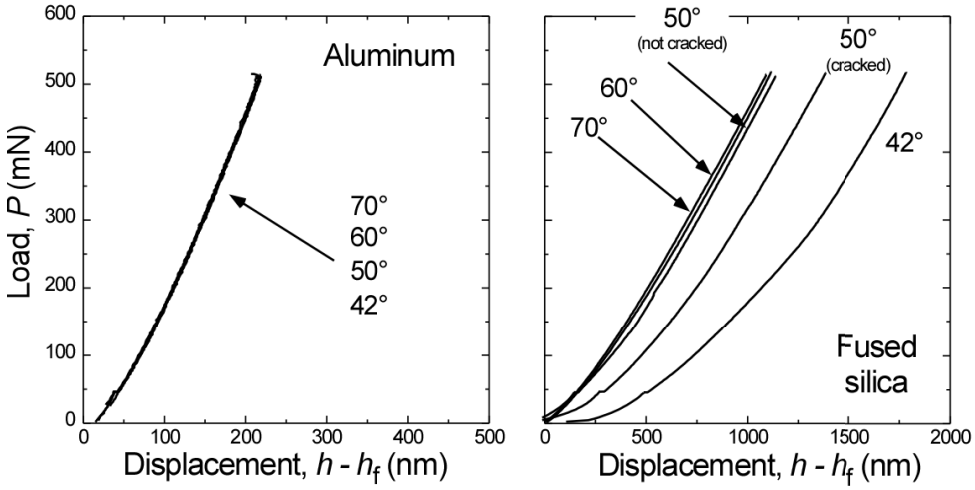

Figure 1. Load as a function of displacement minus final displacement (h-h_f) for four sharp probes on aluminum (left) and fused silica (right). Reproduced from Ref. [9].

The first set of experiments were reported in Morris *et al*. [9]. Four sharp diamond probe indenters were used; the Berkovich, the cube corner, and two 3-sided pyramids of intermediate acuity. The indenters are not referred to by their common names, but by the approximate half-included angle, ϕ, of the axisymmetric equivalent cone. Thus the Berkovich is 70°, the cube-

corner 42°, etc. The materials indented were fused silica and soda-lime glasses, and single crystals of NaCl, BaF_2, Al, and Fe – 3% mass fraction Si. All crystals were $\langle 100 \rangle$-oriented. Indentations were all performed to peak loads of (50, 100, 200, 500 and 700) mN with an indentation strain rate of 0.050 s^{-1} on loading, a 30 s hold at peak load, then unloaded at a constant rate such that 90 % unload was completed in 45 s, and a thermal drift rate calculated before complete unloading. Scanning electron microscopy (SEM) was used to image the residual impressions after indentation.

The relevant results of [9] are quoted here. As expected, the more acute indenters produced more damage at fixed peak load, manifested simultaneously as irreversible work within the load-unload curve, increased pile-up, and fracture at the indentation site. More interestingly, for the three materials (Al, Fe and NaCl) that did not crack, the unloading traces are nearly perfectly superposable. This is shown in Figure 1 for aluminum. When there was radial fracture at the indentation site *and* the indenter was sufficiently acute (50° or 42°) then there was a distortion of the unloading curves away from the obtuse (70° or 60°) indenters. If there was a chance that a particular load-indenter-material combination would or would not fracture, then the unloading curves would either be distorted, or superpose upon Berkovich unloading, depending on whether or not fracture initiated during loading.

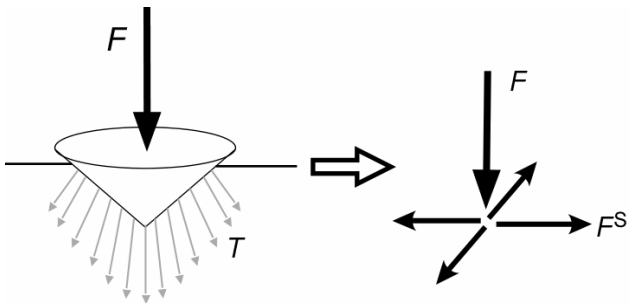

Figure 2. Resolved force F at a rigid conical punch in elastic-plastic indentation results in a traction distribution T that generally will have components normal and tangential to the undeformed surface. The tractions resolve to F and a pair of double forces F^S applied to the half space.

If the experimental results from the instrumented indentation studies are assumed to be widely applicable to homogeneous materials, then the following assertions are made. First, the elastic unloading traces from sharp indentation on uncracked materials are superposable, regardless of indenter acuity. From this, it is concluded that the elastic work done by the probe is (at least for the range of acuity in this experiment) acuity-invariant. Second, radial fracture at the indentation site is a necessary, but insufficient, condition for a compliant distortion of the unloading curve. This suggests that when the indenting probe is sufficiently acute, the effect of radial cracking is to lower the potential energy of the indenting probe; which, by reciprocity, indicates that the elastic stress field of the punch is driving the radial fracture. This is supported by *in-situ* experiments [1] that also show that there is a strong, reversible (and therefore not due to the reaction caused by the plastic deformation) stress field during cube-corner indentation that is weak for the Vickers indenter geometry.

DISCUSSION

Figure 2 is a schematic of elastic-plastic indentation with a sharp indenter. In general the tractions at the contact will not be normal to the undeformed surface. As shown on the right of Figure 2, the traction distributions will resolve in the far-field of the indentation as a point load F and a pair of surface shear double-forces of magnitude F^S. The full displacement and stress fields are known for these simple solutions and are listed in Ref [10]. In fact, the stress field of the

double-forces of magnitude F^{S} is the surface-located blister field [10] and is obtainable by a simple differentiation of the Boussinesq point force solution [11].

A simple model is described below, with the intention of modeling the *far-field* stresses of the indentation as the acuity of the sharp probe increases. By this it is meant that the real boundary conditions at the contact (adhered, finite Coulomb friction or frictionless) are not meant to be captured. While the full stress and displacement fields are known for the point-force solutions shown in Figure 2, the energies are unbounded, and so cannot be used in the energy-balance scheme that follows.

Suppose that there are two individual elastic solutions that produce surface displacement fields u and u' by application, respectively, of surface tractions T_i and T_i' over a common part of the surface *A*. The work required to apply each displacement field individually is denoted by $U(u)$ or $U(u')$; for example,

$$U(u) = \frac{1}{2}\int_A T_i u_i \mathrm{d}A\,. \tag{1}$$

Then, if the tractions of the primed and unprimed displacement fields act simultaneously on *A,* the total strain energy $U(u+u')$ is

$$U(u+u') = U(u) + U(u') + \int_A T_i' u_i \mathrm{d}A\,. \tag{2}$$

A solution is desired such that $U(u+u')$ is unchanged from the reference state $U(u)$. For this to be true,

$$U(u') = \frac{1}{2}\int_A T_i' u_i' \mathrm{d}A = -\int_A T_i' u_i \mathrm{d}A = -\int_A T_i u_i' \mathrm{d}A\,, \tag{3}$$

where the Betti reciprocal theorem has been invoked to form the last term on the right. If unprimed tractions are identified with those corresponding to a frictionless indentation solution, and primed tractions with frictionless axisymmetric outward shear, then Equation (3) forms a basis by which shear tractions may be coupled to normal pressure without changing the elastic work done on the body by the indenting punch. Frictionless pressure and shear solutions are not really necessary, but orthogonal T_i and T_i' simplify the analysis and retain the essential physics.

The reference indentation solution used is isotropic Hertzian contact. Cylindrical coordinates (z, r, θ) are used with the half-space occupying $z \geq 0$. Within the contacted circle of radius *a*, the Hertzian surface tractions T^{H} are a function of normalized radial distance $\rho = r/a$,

$$T^{\mathrm{H}} = \frac{3F}{2\pi a^2}\left(1-\rho^2\right)^{1/2}, \tag{4}$$

where *F* is the total force acting on the punch. The T^{H} produce surface displacements w^{H} normal to the surface and u^{H} tangential to the surface. Now, an axisymmetric shear distribution T^{S} must be chosen to interact with the pressure distribution. Many solutions of this type are available, *e.g.* Ref. [11]; unfortunately, many of the published shear distribution solutions have unbounded energy (typically caused by finite tractions working through infinite displacements). In this work, a new surface shear distribution T^{S} is formed,

$$T^{\mathrm{S}} \propto T^{\mathrm{H}} \frac{1}{a}\frac{\partial}{\partial \rho}\left(w^{\mathrm{H}}\right). \tag{5}$$

This form of T^{S} will fall smoothly to zero at the axis of indentation and at the edge of the contact area. When T^{S} is added to T^{H} in exactly the proportion of Equation (5), this will produce a

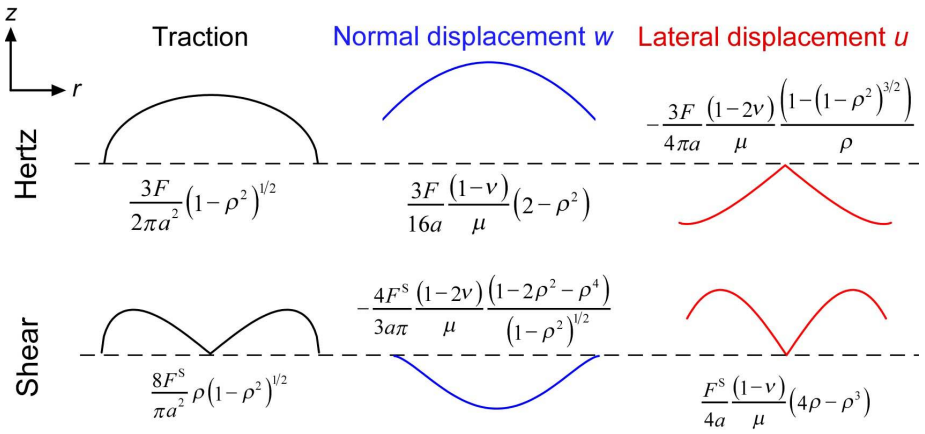

Figure 3. Tractions and displacements for $\rho \le 1$ of the Hertzian solution and shear field of Equation (5). The dashed lines indicate zero.

distribution of surface traction $(T_i + T_i')$ that is normal everywhere to the normal Hertzian displacement field, w^H. From Equations (4) and (5), w and u for the shear tractions are found using the method of Noble and Spence [12]. These, along with the Hertzian tractions and displacements, are listed in Figure 3 as formulas and schematics for easy visualization. The shear force F^S is the vector sum of T^S over π radians, exactly as shown in Figure 2.

In general, addition of the shear tractions to the Hertzian tractions will change the strain energy of the body; but, because each field produces displacements in opposite directions (see Figure 3), the strain energy at fixed load can either be higher, lower or equal to that of the Hertzian field. Equation (3) is a formula that lets one find the magnitude of the shear field that will leave the strain energy unchanged. Substitution of the stresses and displacements in Figure 3 into Equation (3) with Hertzian indentation as the reference solution leads to

$$F^S = \frac{210}{256}\frac{(1-2\nu)}{(1-\nu)}F\,. \qquad (6)$$

Therefore the shear tractions of Equation (5) may be added to the Hertzian field as defined by Equation (6) without changing the strain energy of the body or the force applied to the indenter. The shear force is proportional to the normal force, and is independent of the effective acuity of the indenter. For fixed traction distribution shapes, and fixed interaction surface area (both on the whole of A), this self-similar result is to be expected. Future work will attempt to model indenter acuity effects by breaking the similarity between the shear and pressure fields. There is no energetic difference between frictionless and perfectly adhered indentation for incompressible $(\nu = 1/2)$ materials [13], and Equation (6) reflects this. Radial cracking then is analogous to the effect of slip at the punch face; crack formation relieves shear tractions and leads to punch settlement just as sudden deadhesion at a perfectly bonded punch face would.

CONCLUSIONS

Experiments of nanoindentation by four sharp diamond probes on a set of model materials, ranging in acuity from the Berkovich to the cube-corner, are reexamined. One remarkable result of that study is that elastic unloading load-displacement traces from a common peak load are superposable, except for when there is radial cracking at the indentation site *and*

the indenter is sufficiently acute. Experimental evidence for the wedging mechanism of radial crack development at cube-corner indentations, and not Vickers (or Berkovich) indentations, show that the reversible stress field of the indenting punch changes with acuity. A simple energetic analysis shows that acuity-invariant strain energy and the acuity-dependent wedging effect may be reconciled by adding outward axisymmetric shear to the pressures of indentation in certain proportions. Radial cracking at sufficiently acute indenters will release the forces of surface shear, and this is manifested as a distortion of the unloading curve away from that of an obtuse (*e.g*. Berkovich) indenter. Future work will focus on smoothly capturing the effect of indenter acuity on the stress fields during the entire indentation load-unload cycle.

REFERENCES

[1] D. J. Morris and R. F. Cook, J. Am. Cer. Soc. 87 (2004) 1494.
[2] G. M. Pharr, D. S. Harding and W. C. Oliver, in NATO ASI - Mechanical Properties and Deformation Behavior of Materials Having Ultra-Fine Microstructures, edited by M. Nastasi, D. M. Parkin and H. Gleiter (NATO ASI, 1993) p. 449.
[3] R. F. Cook and G. M. Pharr, J. Am. Cer. Soc. 73 (1990) 787.
[4] B. R. Lawn, A. G. Evans and D. B. Marshall, J. Am. Cer. Soc. 63 (1980) 574.
[5] R. F. Cook and E. G. Liniger, J. Am. Cer. Soc. 76 (1993) 1096.
[6] A. Arora, D. B. Marshall, B. R. Lawn and M. V. Swain, J. Non-Cryst. Solids 31 (1979) 415.
[7] D. J. Morris and R. F. Cook, Int. J. Frac. 136 (2005) 237.
[8] D. J. Morris, A. M. Vodnick and R. F. Cook, Int. J. Frac. 136 (2005) 265.
[9] D. J. Morris, S. B. Myers and R. F. Cook, J. Mater. Res. 19 (2004) 165.
[10] E. H. Yoffe, Phil. Mag. A 46 (1982) 617.
[11] E. H. Yoffe, Phil. Mag. A 54 (1986) 115.
[12] B. Noble and D. A. Spence, Formulation of two-dimensional and axisymmetric problems for an elastic half-space. University of Wisconsin Mathematics Research Center Report #1089, Madison, Wisconsin, (1971).
[13] R. T. Shield and C. A. Anderson, Zeitschrift für Angewandte Mathematik und Physik 17 (1966) 663.